THE JOURNAL OF PHYSICAL CHEMISTRY C

Article

Cite This: J. Phys. Chem. C 2019, 123, 21713−21720

pubs.acs.org/JPCC

# Interaction of Nitroxide Radicals with an $Au_8$ Nanostructure: Theoretical and Calorimetric Studies

Carolina Aliaga,*[,†,‡] Patricio Fuentealba,[‡,§] Francisco Muñoz,[‡,§] Camila Pastenes,[†,‡] Marcos C. Rezende,[†] Evgenia Spodine,[‡,∥] and Carlos Cárdenas*[,‡,§]

[†]Facultad de Química y Biología, Universidad de Santiago de Chile, Casilla 40 Correo 33, 7591538 Santiago, Chile

[‡]Center for the Development of Nanoscience and Nanotechnology, CEDENNA, Av. Ecuador 3493, 9170124 Santiago, Chile

[§]Facultad de Ciencias, Universidad de Chile, Las Palmeras 3425, Ñuñoa, 8320000 Santiago Chile

[∥]Facultad de Ciencias Químicas y Farmacéuticas, Universidad de Chile, Casilla 233, 8320000 Santiago, Chile

**ABSTRACT:** Nitroxide radicals, adhered to gold nanoparticles, have found novel applications such as cancer treatment, neuroprotection after cerebral injury, radiotherapy, and as drug-delivering agents. The details of the nature of the binding of nitroxide radicals to metallic nanostructures have been a subject of debate for the last two decades. In this work, microcalorimetric measurements are complemented with a theoretical study of noncovalent interactions between different derivatives of the nitroxide radical 2,2,5,5-tetramethylpiperidinoxyl and an $Au_8$ nanocluster to shed light on the nature of the binding of the radical molecule and the nanocluster. Experiments and theory showed that, although the molecule could bind through the nitroxide group, organic substituents such as amino and carboxyl groups interact much more favorably with the nanocluster. Attachment of these groups to the gold nanocluster is the result of an intense polarization of the "nucleophilic" sites of the metallic cluster, strengthened by van der Waals attraction between the molecule and the nanocluster.

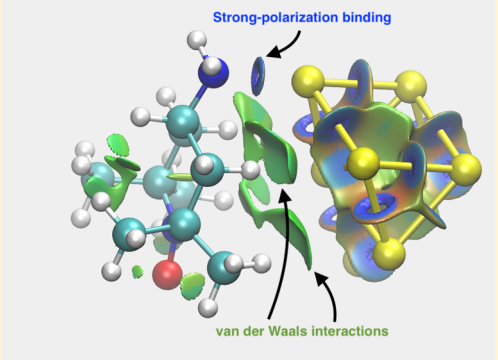


## INTRODUCTION

Nitroxide radicals find various applications in organic synthesis and polymer chemistry.[1] As scavengers of reactive oxygen species, their use with metallic nanocarriers has led to the development of new tools for cancer treatment.[2] Radical-containing nanoparticles have been employed to deliver nitroxides for neuroprotection after cerebral injury.[3] Besides, the fact that gold is itself a good absorber of X-rays makes gold nanoparticles (AuNPs) important aids in radiotherapy treatment[4] and in drug-delivery systems.[5]

A proper understanding of their association with different nanosystems has therefore been the goal of many research studies, emphasizing, for example, the development of more efficient drug carriers,[6] the development of prefluorescent sensors for antioxidants in biological media,[7,8] or focusing more specifically on the nature of their binding to the metallic surface. The details of the nature of their binding to metallic nanostructures have been a subject of debate for the last two decades.[7−13] The initial suggestion that there was a direct interaction between the nitroxide group and AuNPs, based on EPR measurements of 2,2,6,6-tetraethylpiperidineoxyl (TEMPO) radical derivatives in the presence of AuNPs,[9] was later developed in a study of the fluorescence quenching of gold nanoclusters (AuNCs) by 4-aminoTEMPO, leading the authors to postulate a direct binding between the metal surface and the nitroxide oxygen.[8]

Such a direct binding found support in some works that investigated the interaction of nitroxide radicals with AuNPs by means of far infrared (IR) spectroscopy[12] and X-ray photoelectron spectroscopy analysis.[10] However, indirect evidence from studies of the quenching of CdSe quantum dots (QDs) by TEMPO and the 4-aminoTEMPO radicals shed some doubt on the existence of such a direct binding between the $NO^{\bullet}$ fragment and the metal surface. Although a direct binding was postulated for the 4-aminoTEMPO radical, the authors concluded that no such binding existed for the unsubstituted TEMPO radical.[11] Studies on the fluorescence quenching of CdSe QDs by adsorbed functionalized TEMPO derivatives led to a similar conclusion: a strong binding existed between either an amino or a carboxylic substituent of the radical and the metal surface but not with the nitroxide group.[14]

A comparison of the ability of 4-amino- and 4-hydroxyTEMPO to quench the fluorescence of CdTe QDs led to the conclusion that, unlike the 4-amino derivative, which formed a nonfluorescent conjugate with the metal surface, 4-hydroxyTEMPO could only quench the QD fluorescence by collision.[15]

**Received:** April 15, 2019
**Revised:** August 6, 2019
**Published:** August 17, 2019






DOI: 10.1021/acs.jpcc.9b03422
J. Phys. Chem. C 2019, 123, 21713−21720

These conflicting reports from the literature on the nature of the binding between a nitroxide radical and its derivatives with a metallic nanostructure led us to investigate, with the aid of EPR, fluorescence, kinetics, electronic microscopy and, calorimetric measurements, the interaction of four TEMPO derivatives with AuNCs. Our conclusion was that although a direct binding between the nitroxide fragment of these TEMPO radicals and the gold surface could not be ruled out, it was negligible if compared with alternative bindings between the metal surface and substituents like $NH_2$ or $CO_2H$.[16]

Our main evidence for such a conclusion was drawn from TEM images of 4-amino- and 4-carboxyTEMPO radicals adsorbed on the surface of AuNC and from calorimetric measurements of the exothermic binding between these TEMPO derivatives and AuNC, practically absent in the case of 4-hydroxyTEMPO and unsubstituted TEMPO.

In the present communication, we resorted to theoretical calculations and new experiments to gain a deeper insight into the nature of the interactions between an AuNC and the radical TEMPO derivatives **1**−**4** (Scheme 1).

**Scheme 1. Nitroxide Radicals Studied in This Work**

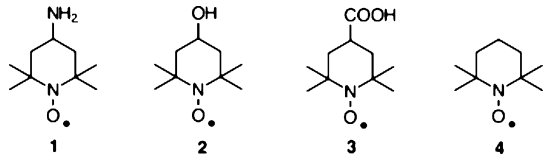


Theoretical calculations on the interactions of various AuNCs with organic species can be found in the literature for a variety of ligands. Some examples include propene binding to small gold clusters,[17] the interaction of pyridine derivatives with a gold (111) surface,[18] the interactions of guanine derivatives,[19] imidazole,[20] thiolate, chloride, and phosphine ligands[21] of peptides[22] and PAMAM dendrimers[23] and benzimidazole-2-ylidenes[24] with $Au_n$ clusters.

Such calculations have focused on the distribution of charge among the clustered gold atoms and their interaction with a given ligand,[19,21,23,24] or with the frontier molecular orbitals of the isolated cluster, or of the ligand adsorbed on the metallic surface.[19,21−23] The stability and reactivity of various conformers of $Au_n$ ($n$ = 6−13) were compared using density functional theory-based reactivity descriptors such as the Fukui functions, which allows the identification of available sites for a nucleophilic and/or electrophilic attack on the clusters.[25] Calculations favored planar conformations as the most stable for small clusters ($Au_6$−$Au_9$), although previous experimental evidence from IR spectral measurements suggested that different conformations for a given cluster probably coexisted in solution.[26] Geometrical optimizations of the adsorbed ligands on the metallic clusters yielded clear pictures for their interaction, leading also to estimate their binding energies.[18−21,23,24] These theoretical works validate the use of density functional theory (DFT) to characterize the interaction between organic molecules and AuNPs.

In the present study of the regioselective interactions of **1**−**4** with an AuNC, we decided to use the reduced gradient of the density as a noncovalent interaction (NCI) index[27,28] for the identification of all NCIs in the AuNC−ligand supermolecules.

After identifying, from calculations of Fukui functions[25,29] for a AuNC, the regions prone to nucleophilic and/or to electrophilic attack, we matched these regions with the nucleophilic and/or electrophilic centers in ligands **1**−**4** in order to have an educated guess of the interaction between the ligands and nanocluster.[30] The predicted binding enthalpies of the resulting supermolecules were compared with the relative experimental calorimetric measurements of compounds **1**−**4** with AuNCs[16] and with new measurements of analogous compounds with the same AuNCs under the same experimental conditions. Finally, an explanation of the binding enthalpies was given in terms of the NCI.

The results presented here settle past controversial views regarding the details of the nature of the binding of nitroxide radicals with AuNPs. By quantifying such interactions with the aid of calorimetric measurements and supporting these experimental values with theoretical calculations, they provide a fine and detailed picture of how the interactions with an AuNC take place, not only with the NO$^\bullet$ fragment but also with other functional groups present in an organic ligand.

## EXPERIMENTS AND CALCULATIONS

Calorimetric measurements were carried out with an isothermal titration calorimeter MicroCal ITC from TA Instruments. All measurements were carried out at 25 °C. Solutions of citrate-coated AuNCs with an average diameter of ca. 0.7 nm were prepared and characterized as previously described.[16] Calorimetric profiles were obtained by incremental titration (2.5 $\mu$L every 400 s) of aqueous solutions of the ligand into a 170 $\mu$L aqueous solution of the AuNC, stirred at 350 rpm. For the treatment of the data, the AuNC (assumed equal to 1 $\mu$M) and the ligand concentrations were fed into the ITC software, which converts the experimental calorimetric profile into a sigmoidal plot of peak areas (enthalpy) against the mole ratio of the two interacting species.

Theoretical calculations employed the Gaussian 09 package.[31] All geometry optimizations were performed within the unrestricted Kohn−Sham DFT formalism using the long-range corrected hybrid density functional of Head-Gordon et al.[32,33] $\omega$B97X-D and the split-double-valence basis set 6-31+G(d,p) for atoms of the main group. For Au, 60 core electrons are replaced by a Stuttgart effective core potential with relativistic scalar corrections.[34] For the valence electrons, a split-double-valence basis set, designed to be used with the pseudopotential, was used.[35] The $\omega$B97X-D functional was chosen because it is a hybrid functional with range separation that employs 100% of Hartree−Fock-type exchange (EXX) for the long-range electron−electron interaction, which also includes empirical dispersion effects (van der Waals corrections).[36] The advantage of this functional is that it recovers the correct long-range $1/r$ behavior of the exchange potential, while its computational cost is similar to standard functionals. Having a correct description of the dispersion effects is essential to describe weak interactions between molecules and the gold cluster. Besides, $\omega$B97X-D has the advantage of reproducing well the properties of small metallic clusters and organic molecules.[37]

All optimized geometries were confirmed to be stationary points through vibrational frequency analysis. To compute enthalpies, the partition functions were split into translational, rotational, and harmonic-vibrational parts.[38]

Because the frontier orbitals of $Au_8$ are degenerated, we computed its Fukui functions for nucleophilic ($f^+(\mathbf{r})$) and electrophilic attack ($f^-(\mathbf{r})$) within the frozen orbital-state-averaged approximation.[39−41] In short, $f^+(\mathbf{r})$ is large in regions



DOI: 10.1021/acs.jpcc.9b03422
J. Phys. Chem. C 2019, 123, 21713−21720

where the cluster is prone to accept electrons, while large $f^-(\mathbf{r})$ values correspond to regions where the cluster is prone to donate electrons.

In order to distinguish all interactions that occur between the cluster and ligands, a NCI analysis was carried out.[27,28] The NCI analysis is based on the empirical fact that the reduced density gradient (RDG, eq 1) shows low-value peaks in regions of low electron density, $\rho(\mathbf{r})$, associated to dispersion interactions, hydrogen bonds, strong polarization, and steric clashes.

$$\mathrm{RDG}(\mathbf{r}) = 2^{-1}(3\pi^2)^{-1/3}\frac{|\nabla\rho(\mathbf{r})|}{\rho(\mathbf{r})^{4/3}} \quad (1)$$

The type of interaction can be distinguished by the sign of the second largest eigenvalue of the Hessian of the density, $\lambda_2$. A positive value indicates depletion of the density, that is, repulsive steric interactions. A negative value indicates aggregation of the density, that is, attractive interactions, such as hydrogen bonds, and interactions mediated by polarization. The value of $\lambda_2\rho(\mathbf{r})$ can be slightly positive or negative in regions of very low density, indicating dispersion interactions. RDG and $\lambda_2$ values were calculated with Chemtools and Horton.[42]

## RESULTS AND DISCUSSION

An AuNC with 8 atoms was chosen as a model for the nanoparticles. This size corresponds to the aggregation number of atoms of the isolated smallest particles[38] revealed by dynamic light scattering (DLS)[16] (see Figure 1c). The geometry of the most stable $Au_8$ cluster is still a matter of debate among theoreticians.[43,44] It seems that a planar cluster is slightly more stable in the gas phase than nonplanar conformations. The $Au_8$ cluster employed in this work corresponds to the most stable nonplanar conformer with a $C_{2v}$ symmetry (Figure 1). We preferred to use this three-dimensional structure over the 2-D because measurements suggested the existence of spherical particles for our citrate-coated AuNC[16] and because a chelated nonplanar structure should plausibly be more stable in solution than a planar conformer.[45]

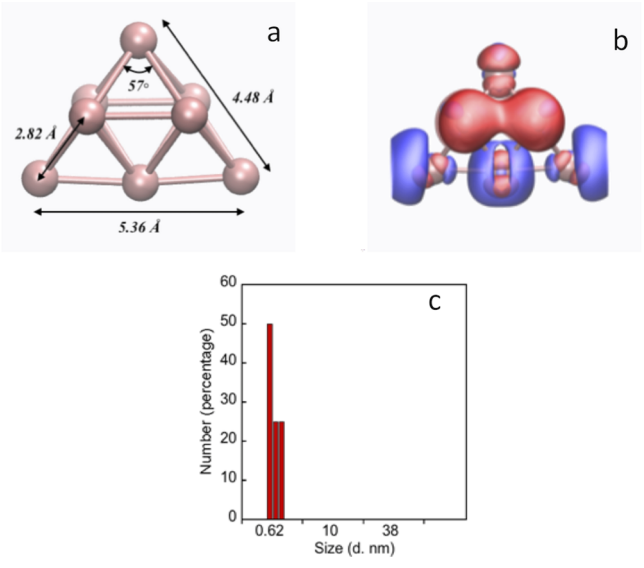


**Figure 1.** (a) Three-dimensional structure of the $Au_8$ cluster employed in this work. Sticks are only visual guides and are not to be understood as directional chemical bonds. (b) Isosurfaces of the electrophilic (in red) and nucleophilic (in blue) Fukui functions of the cluster $Au_8$. Both isosurfaces correspond to values of $f^+(\mathbf{r}) = 0.0005 a_0^{-3}$. (c) Particle-size distribution of the citrate-coated AuNC, determined by DLS.

In order to define the starting geometries for the $Au_8$–ligand supermolecules, the nucleophilic functional groups of **1**–**4** were placed close to the vertex atom where $f^+(\mathbf{r})$ is large (blue lobes in Figure 1b), while electrophilic centers were placed close to one of the equivalent central atoms where $f^-(\mathbf{r})$ was large (red lobes in Figure 1b). It should be kept in mind, however, that the high polarizability of metallic clusters makes this differentiation less clear than in organic molecules. Hence, whenever the optimization suggested several stable isomers, all of them were investigated, and the one with the lowest energy was chosen for the analysis.

**Interactions between the $Au_8$ and the TEMPO Derivatives.** Table 1 lists all the calculated enthalpies for the supermolecules formed by the $Au_8$ nanocluster and the TEMPO derivatives. For the sake of comparison, three other ligands had their binding enthalpies with the AuNC included in Table 1. None of these ligands (cyclohexylamine, cyclohexanol, and cyclohexanecarboxylic acid) presented any ambiguity as to the site of their interaction with the AuNCs: the amino, hydroxyl, or the carboxyl groups, respectively. The table also includes the calculated binding energy with benzoic acid. As shown below, a significant variation was observed in the binding values of cyclohexanecarboxylic and benzoic acid. NCI analysis not only reproduced this difference but also revealed the causes for their different behavior because of subtle differences of their $Au_8$–ligand geometries.

**Table 1. Calculated Binding Enthalpies (kJ $mol^{-1}$) of the TEMPO Derivatives 1–4 and of Four Related Ligands (Cyclohexylamine, Cyclohexanol, Cyclohexanecarboxylic Acid, and Benzoic Acid) with the $Au_8$ Nanocluster**

| | site of interaction | | | |
|---|---|---|---|---|
| Ligand | $NH_2$ | OH | $CO_2H$ | $NO^\bullet$ |
| **1**[a] | −92.8 | | | −61.2 |
| **2**[a] | | −69.8 | | −65.0 |
| **3**[a] | | | −84.9 | −65.2 |
| **4**[a] | | | | −68.6 |
| Cyclohexylamine | −114.9 | | | |
| Cyclohexanol | | −74.8 | | |
| cyclohexane-carboxylic acid | | | −81.5 | |
| benzoic acid | | | −72.0 | |

[a]Enthalpy values refer to the conformer with the smallest value.

The structure and isosurfaces of the RDG (0.4) of $Au_8$ bound to radicals **1**–**4** through the $NO^\bullet$ fragment are shown in Figure 2. Isosurfaces describe regions of steric clashes (red), attractive dispersion (green), and stronger attractive (blue) interactions. These stronger attractive interactions arise from polarization of the electron densities. Among the three types of interactions mentioned above, the density is higher in regions of stronger interaction (blue) ($\rho(\mathbf{r}) \geq 4.0 \times 10^{-2}\ a_0^{-3}$). Attractive dispersion shows up at smaller value of density, $\rho(\mathbf{r}) \leq 1.5 \times 10^{-3}\ a_0^{-3}$, and positive and negative $\lambda_2$. In all cases, the strongest interactions occur between the $NO^\bullet$ fragment and the same metallic "electrophilic" atom in $Au_8$. The Au–O binding enthalpy is the same for all TEMPO derivatives, except



DOI: 10.1021/acs.jpcc.9b03422
J. Phys. Chem. C 2019, 123, 21713−21720

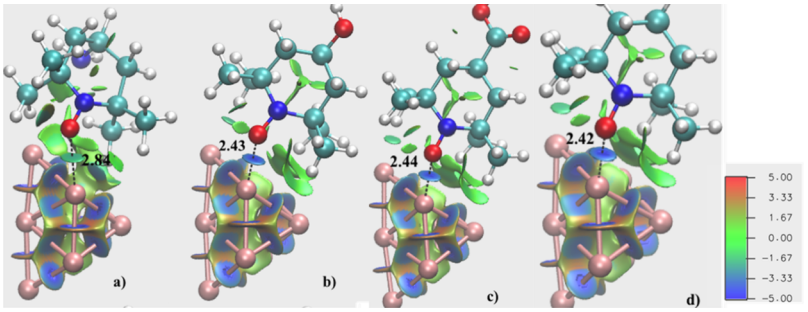


**Figure 2.** Structures and reduced density-gradient isosurfaces (0.4) of TEMPO derivatives **1** (a), **2** (b), **3** (c), and **4** (d) interacting with $Au_8$ through the $NO^{\bullet}$ fragment. Isosurfaces describe regions of steric clashes (red), attractive dispersion (green), and stronger attractive interactions (blue). 100 $\text{sign}(\lambda_2)\rho(\mathbf{r})$ values are indicated alongside the color scale. Distances are in angstroms.

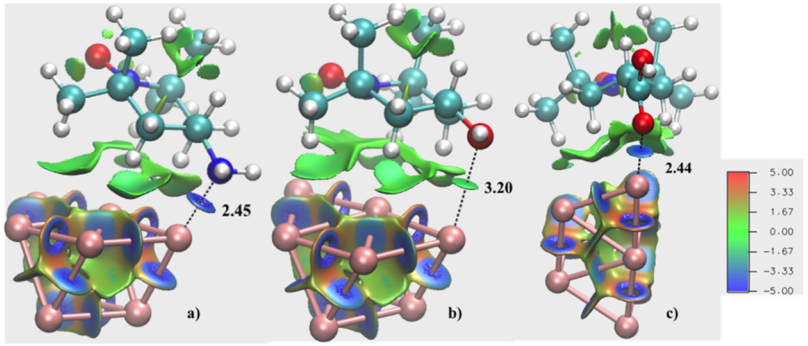


**Figure 3.** Structures and reduced density-gradient isosurfaces (0.4) of TEMPO derivatives **1** (a), **2** (b), and **3** (c) interacting with $Au_8$ through the 4-substituent. Isosurfaces describe regions of steric clashes (red), attractive dispersion (green), and stronger attractive interactions (blue). 100 $\text{sign}(\lambda_2)\rho(\mathbf{r})$ values are indicated alongside the color scale. Distances are in angstroms.

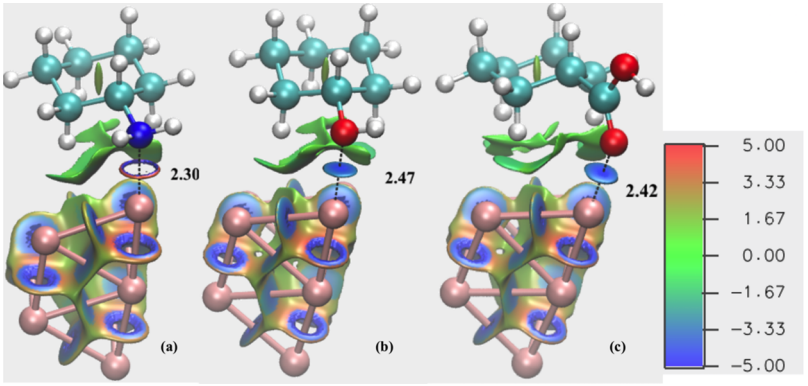


**Figure 4.** Structures and reduced density-gradient isosurfaces (0.4) of cyclohexylamine (a), cyclohexanol (b), and cyclohexanecarboxylic acid (c) interacting with $Au_8$. Isosurfaces describe regions of steric clashes (red), attractive dispersion (green), and stronger attractive interactions (blue). 100 $\text{sign}(\lambda_2)\rho(\mathbf{r})$ values are indicated alongside the color scale. Distances are in angstroms.

for compound **1** (Table 1). In this case, the local attraction is stronger than a dispersion interaction but smaller than the polarization of the electron density observed for compounds **2**−**4**. This result agrees with the corresponding Au−O distance, which is clearly larger for derivative **1** (2.8 Å), than for the other compounds (≈2.4 Å). The NCI analysis also agrees with the smaller binding enthalpy of derivative **1**. Dispersion interactions contribute to a smaller extent to the binding of the $NO^{\bullet}$ fragment to the nanoparticle. Figure 2b,d shows similar Au−O distances for compounds **2** and **4**, but regions of van der Waals interactions are slightly larger for derivative **4**, in agreement with a larger binding enthalpy for the latter.

Figure 3 shows the structure and equivalent isosurfaces of the RDG for TEMPO derivatives **1**−**3** bound to $Au_8$ through their 4-substituents. The most favorable interaction now happens with the "nucleophilic" region of the cluster. Binding of the amino and carboxyl groups to the nanoparticle originates from a strong polarization of the electron density (deep-blue). Comparison with Figure 2 shows that the interaction between the $Au_8$ and the substituent groups of **1** and **3** is stronger than with the $NO^{\bullet}$ fragment. This is in agreement with the $-NH_2$ and $-CO_2H$ groups having the largest computational binding enthalpies, −92.8 and −84.9 kJ $mol^{-1}$ respectively (see Table 1).

By contrast, the 4-hydroxyTEMPO **2** shows a much weaker binding than **1** or **3**, reflecting a dispersion interaction (green)



DOI: 10.1021/acs.jpcc.9b03422
J. Phys. Chem. C 2019, 123, 21713−21720

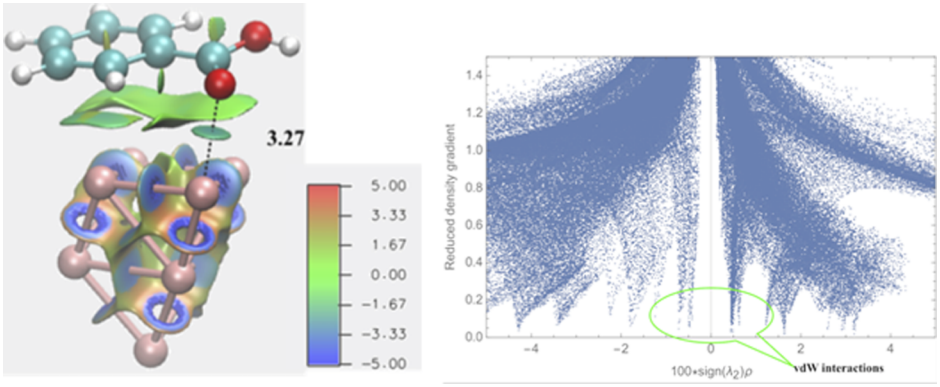


**Figure 5.** Left: Structure and reduced density-gradient isosurfaces (0.4) of benzoic acid interacting with $Au_8$. Isosurfaces describe regions of steric clashes (red), attractive dispersion (green), and stronger attractive interactions (blue). 100 sign($\lambda_2$)$\rho$(**r**) values are indicated alongside the color scale. Distances are in angstroms. Right: Scatter plot of the reduced density gradient vs 100 sign($\lambda_2$) $\rho$(**r**). The peaks around $\rho(\mathbf{r}) \approx 5 \times 10^{-4}$ $a_0^{-3}$ correspond to a van der Waals interaction between the aromatic ring of the molecule and the cluster.

with the nanoparticle. Comparison with Figure 2 shows that this interaction is weaker than the Au−O interaction with the NO• fragment (blue). The corresponding distances confirm this: 2.43 Å for the Au−O with the NO• fragment and 3.40 Å for the Au−O with the OH substituent. Note that, in this case, the values of the binding enthalpies of Table 1 (−65.0 kJ $mol^{-1}$ for NO• and −69.8 kJ $mol^{-1}$ for OH) do not correlate with Au−O distances because interactions occur with different Au atoms in the cluster.

Finally, we have also performed NCI analysis of the cluster interacting with cyclohexylamine, cyclohexanol, and cyclohexanecarboxylic acid. Figure 4 shows that the distances between the AuNC and the adatoms of the ligands increase in the order $-NH_2$ < $-OH$ < $-CO_2H$. This order reflects the binding enthalpies of the three reference ligands with the $Au_8$ listed in Table 1.

Interestingly, and in agreement with the calculated enthalpies of Table 1, NCI analysis revealed substantial differences between the two ligands, cyclohexanecarboxylic and benzoic acid. However with cyclohexanecarboxylic acid, there is a strong polarization interaction between the carboxy group and the cluster (Figure 4c), and most of the binding with benzoic acid (Figure 5) originates from strong van der Waals interactions between the aromatic ring, the carboxy group, and the clusters. The difference between both interactions becomes clear in a plot of the RDG versus sign($\lambda_2$)$\rho$(**r**). While the strong interaction peak in the RDG of the supermolecule with cyclohexanecarboxylic acid corresponds to densities higher than $5.0 \times 10^{-2}$ $a_0^{-3}$, with benzoic acid, and the density is considerably lower, less than $1.0 \times 10^{-3}$ $a_0^{-3}$, in the intermediate region between the aromatic ring and the cluster. These low-density values, associated with van der Waals interactions, explain the larger distance between the $Au_8$ and the $-CO_2H$ group (3.27 vs 2.42 Å, for benzoic vs cyclohexanecarboxylic acid respectively) (Figures 4c and 5), and consequently the smaller binding enthalpy with benzoic acid (Table 1).

The above theoretical results thus confirmed our previous conclusion that binding of the 4-amino- or the 4-carboxy-TEMPO radicals with the AuNC takes place through the 4-substituent and not through the NO• fragment. Calorimetric measurements had also suggested similarly negligible binding energies of the unsubstituted TEMPO or the 4-hydroxyTEMPO radical with the AuNC, when compared with the interactions of derivatives **1** and **3**.[16] This is also shown in Table 1, where the calculated binding energies of the NO• fragment and the 4-OH substituent with the AuNC are very similar and smaller than the binding energies with the carboxy or the amino groups. These results are in agreement with observations from literature that ligands such as PAMAM-OH dendrimers, with a terminal hydroxyl group, perform poorly as stabilizers of AuNPs.[23]

An interesting feature from the structures of Figures 2 and 3 is that the TEMPO ligands sit differently on the AuNC, depending on the group that interacts with the surface. The ligand lies nearly perpendicular to the AuNC when it binds through the NO• fragment (Figure 2), lying flat when it binds through the 4-substituent (Figure 3). Although the major interaction with the metallic cluster takes place via the 4-substituent, the dispersion interaction of the ring and the NO• fragment with the cluster seems to be responsible for the observed inclination of the ligand, which lies with its ring bent toward the metallic surface. Nearly 20 years ago, Levanon, Meisel et al. speculated for the first time on the interaction of nitroxide radicals with AuNPs, suggesting that 4-amino-TEMPO **1** "adsorbs flat parallel to the (metal) surface".[9] The structure shown in Figure 3a gives support to this suggestion. It also points to a more complex interaction between the 4-substituted radical and the $Au_8$ cluster, where both nucleophilic and electrophilic centers in the two partners interact to form a stable grafted nanoparticle.

**Comparison with Calorimetric Results.** Validation of the theoretical results described above was sought with experimental binding energies estimated from microcalorimetric measurements. Previous estimates of the relative binding enthalpies of **1**−**4** with a citrate-capped AuNC in water relied on the arbitrary assumption that the AuNC solutions had a cluster concentration of 1 $\mu$M.[16] Under these conditions, the obtained binding enthalpies are not absolute. However, if all measurements are performed under the same conditions, relative values of the obtained enthalpies can be used to compare the affinities of the different ligands for the same nanocluster. Enthalpies can be obtained from sigmoidal plots of the integrated peak areas, corresponding to corrected heat rates versus the ratio of the two-binding species. In these plots, the molar ratio at the center of the sigmoidal isotherm corresponds to the reaction stoichiometry. In addition, the enthalpy is also derived from the isotherm, as the amount of


DOI: 10.1021/acs.jpcc.9b03422
J. Phys. Chem. C 2019, 123, 21713−21720

heat released per mole of ligand bound. In this way, the relative binding enthalpies of the three reference ligands—cyclohexylamine, cyclohexanol, and benzoic acid—could be compared with those of TEMPO derivatives **1**−**3**. Examples of the calorimetric pattern obtained for these reference ligands under the same conditions and the same AuNC solution are reproduced in Figure 6. The obtained binding enthalpies for all ligands are listed in Table 2.

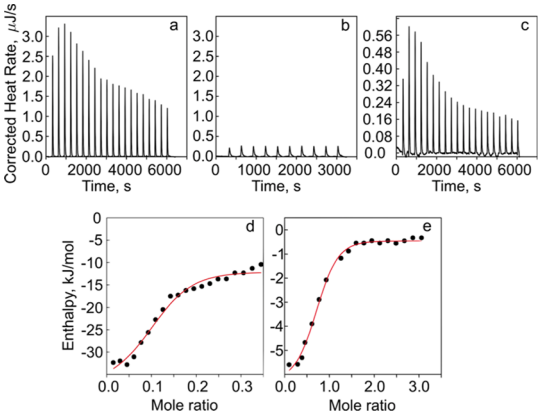


**Figure 6.** Calorimetric profiles for the addition of 50 μL aqueous solutions of 1.0 mM of cyclohexylamine (a), 1 mM of cyclohexanol (b), and 0.5 mM of benzoic acid (c) to 170 μL of an aqueous solution of the AuNC. ITC conditions were as follows: stirring 350 rpm and syringe volume 50 μL. Injected volume in each pulse: 2.5 μL and interval between injections: 400 s. Sigmoidal titration curves for cyclohexylamine (d) and benzoic acid (e) obtained from the calorimetric profiles.

**Table 2. Microcalorimetric Estimates of Binding of TEMPO Derivatives 1−4 or of the Related Ligands Cyclohexylamine, Cyclohexanol, Cyclohexanecarboxylic Acid, and Benzoic Acid, with a Citrate-Capped AuNC in Water**

| ligand | binding enthalpy[a]/kJ mol$^{-1}$ |
|---|---|
| 4-aminoTEMPO **1** | −89.2[b] |
| 4-hydroxyTEMPO **2** | <1[b] |
| 4-carboxyTEMPO **3** | −12.6[b] |
| TEMPO **4** | <1[b] |
| cyclohexylamine | −100 |
| cyclohexanol | <1 |
| cyclohexanecarboxylic acid | −71.9 |
| benzoic acid | −12.6 |

[a]Assuming an AuNC concentration of 1 μM. [b]Data from ref 16.

Comparison of the binding enthalpies of the reference ligands with those of the TEMPO derivatives **1**−**4** leaves little doubt as to the nature of the groups that bind to the metallic surface: the amino group in cyclohexylamine and in **1**, with close enthalpy values (−100 and −89.2 kJ mol$^{-1}$, respectively) binds more effectively than the carboxy group in cyclohexanecarboxylic acid and in **3** (−71.9 and −12.6 kJ mol$^{-1}$, respectively). The hydroxyl group in cyclohexanol and in 4-hydroxyTEMPO binds negligibly to the AuNC, similarly to the NO$^{\bullet}$ fragment of the unsubstituted TEMPO **4**, all with an enthalpy smaller than 1 kJ mol$^{-1}$.

The above trends agree qualitatively with the theoretical results summarized in Table 1.

However, significant quantitative departures are observed when the values of the theoretical binding energies of Table 1 of the TEMPO derivatives **1**−**4** are compared with the corresponding enthalpies of Table 2. In general, theory predicts reasonably close binding energies with the $Au_8$ cluster for the four fragments in the gas-phase process: $NH_2$ (−92.8 kJ mol$^{-1}$) < $CO_2H$ (−84.9 kJ mol$^{-1}$) < OH (−69.8 kJ mol$^{-1}$) ≈ NO$^{\bullet}$ (−68.6 kJ mol$^{-1}$). In water and in the presence of a citrate-capped AuNC, these values are somewhat different: $NH_2$ (−89.2 kJ mol$^{-1}$) < $CO_2H$ (−71.9 kJ mol$^{-1}$) < OH (<1 kJ mol$^{-1}$) ≈ NO$^{\bullet}$ (<1 kJ mol$^{-1}$). Binding values with the $NH_2$ and with the $CO_2H$ groups show a fairly good agreement with gas-phase calculations, but this is not observed for the bindings with the OH and the NO$^{\bullet}$ groups. An explanation for these discrepancies may be sought in the gold cluster and in the solvent. If the affinities of an −OH group and of a NO$^{\bullet}$ fragment for $Au_8$ are very similar, as shown by the theoretical results of Table 1, both ligands **2** and **4** and cyclohexanol should compete very poorly with the water molecules that solvate a citrate-capped gold cluster, leading to negligible heat variations upon addition of any of the two ligands to an aqueous AuNC solution.

The reduced binding enthalpy of the carboxylic group of **3** in water (−12.6 kJ mol$^{-1}$), compared with the theoretical value in the gas-phase (−84.9 kJ mol$^{-1}$), can also be explained by consideration of the cluster-stabilizing citrate-capping in this solvent. Replacing a carboxylic acid ligand by another carboxylic acid should require larger concentrations of the added ligand to displace the equilibrium in solution. This should correspond to a diminished binding enthalpy in solution, compared to the one computed with the naked gold cluster.

The calorimetric results also reproduce the theoretical trends observed in Table 1, regarding the two carboxylic acid ligands. Binding values of the two analogous acids (cyclohexanecarboxylic and benzoic acid) were rather different, with a diminished binding enthalpy of the aromatic ligand (−12.6 kJ mol$^{-1}$) vis-à-vis its aliphatic analogue (−71.9 kJ mol$^{-1}$). These calorimetric measurements are in qualitative agreement with the corresponding calculated binding energies of Table 1 (−72.0 kJ mol$^{-1}$ for benzoic acid and −81.5 kJ mol$^{-1}$ for cyclohexanecarboxylic acid). The explanation for these differences, based on the NCI analysis of the two supermolecules (Figures 4c and 5), is thus reinforced by the experimental results of Table 2.

The result of this additional parallel interaction of the ligand with the metallic surface is also evident if the bindings of the TEMPO derivatives **1** and **3** are compared with those of their homocyclic analogues, cyclohexylamine and cyclohexanecarboxylic acid, respectively. Although in all cases, a direct binding is postulated between the AuNC and the functional group ($NH_2$ or $CO_2H$), TEMPO derivatives **1** and **3** bind less strongly with AuNC than their homocyclic analogues. This experimental trend is confirmed by the theoretical calculations. The possible cause for this is the additional parallel interaction of the ligand with the metallic surface, which is present with the TEMPO ligands but not with cyclohexylamine or cyclohexanecarboxylic acid. Such an interaction, described as an attractive dispersion in Figures 3−5, has the effect of weakening the stronger attraction between the nucleophilic substituent and the metallic surface, so that the Au−$NH_2$ bond-length formed with cyclohexylamine (2.30 Å in Figure 4a) increases to 2.45 Å with the 4-aminoTEMPO ligand (Figure 3a). The same effect is observed when the TEMPO ligand **3** is compared with the homocyclic cyclohexanecarbox-


DOI: 10.1021/acs.jpcc.9b03422
J. Phys. Chem. C 2019, 123, 21713−21720

ylic acid. The Au−$CO_2H$ bond length in the former (2.44 Å in Figure 3c) decreases to 2.42 Å in the Au−cyclohexanecarboxylic supermolecule (Figure 4c)

## CONCLUSIONS

The interaction of the nitroxide radical 2,2,5,5-tetramethylpiperidinoxyl (TEMPO) and three of its 4-substituted derivatives (4-amino-, 4-hydroxy-, and 4-carboxyTEMPO) and four related ligands, (cyclohexylamine, cyclohexanol, cyclohexanecarboxylic acid, and benzoic acid), with an $Au_8$ nanocluster was studied theoretically and experimentally. All theoretical and experimental results showed that, for the series of TEMPO derivatives **1**−**4**, 4-aminoTEMPO binds most strongly with the $Au_8$ cluster, followed by 4-carboxyTEMPO, and that binding with the gold cluster takes place through the 4-substituent. The affinities of the 4-OH group and of the $NO^•$ fragment for $Au_8$ were very similar but smaller than those of the amino or carboxy groups, in agreement with the negligible binding enthalpies obtained for TEMPO and 4-hydroxyTEMPO with the citrate-capped AuNC. Nevertheless, the structure of the 4-aminoTEMPO ligand grafted onto the $Au_8$ cluster deviated from a purely vertical alignment of the piperidinoxyl ring with the metallic surface, suggesting that dispersion interactions of the ring and the $NO^•$ fragment contribute significantly to the binding, being responsible for the inclination of the ligand. Thus, our results lend some support to a previous speculation on the nature of the interactions between 4-aminoTEMPO and AuNCs, as arising from this ligand sitting flat parallel on the metallic surface.[9]

In conclusion, by coupling microcalorimetric measurements with the theoretical characterization of NCI in supermolecules, a consistent picture was obtained, leading to a better understanding of the interactions between an AuNC and different organic ligands, which can be possibly applied to other nanosystems.

## AUTHOR INFORMATION


### Corresponding Authors

*E-mail: carolina.aliaga@usach.cl (C.A.).
*E-mail: cardena@uchile.cl (C.C.).

### ORCID

Carolina Aliaga: 0000-0002-1352-3164
Marcos C. Rezende: 0000-0003-2040-9009
Carlos Cárdenas: 0000-0002-0648-6502


### Notes

The authors declare no competing financial interest.

## ACKNOWLEDGMENTS

We are grateful to CONICYT grant FB0807 and also to FONDEQUIP project EQM140174 and to Jaime Huerta. C.A., C.C. and P.F. thank FONDECYT projects 1160486, 1181121 and 1180623, respectively. This research was partially supported by the supercomputing infrastructure of the NLHPC (ECM-02).

## REFERENCES


(1) Tebben, L.; Studer, A. Nitroxides: Applications in Synthesis and in Polymer Chemistry. *Angew. Chem., Int. Ed.* **2011**, *50*, 5034−5068.
(2) Yoshitomi, T.; Hirayama, A.; Nagasaki, Y. The ROS Scavenging and Renal Protective Effects of PH-Responsive Nitroxide Radical-Containing Nanoparticles. *Biomaterials* **2011**, *32*, 8021−8028.
(3) Marushima, A.; Suzuki, K.; Nagasaki, Y.; Yoshitomi, T.; Toh, K.; Tsurushima, H.; Hirayama, A.; Matsumura, A. Newly Synthesized Radical-Containing Nanoparticles Enhance Neuroprotection after Cerebral Ischemia-Reperfusion Injury. *Neurosurgery* **2011**, *68*, 1418−1426.
(4) Hainfeld, J. F.; Dilmanian, F. A.; Slatkin, D. N.; Smilowitz, H. M. Radiotherapy Enhancement with Gold Nanoparticles. *J. Pharm. Pharmacol.* **2008**, *60*, 977−985.
(5) Duncan, B.; Kim, C.; Rotello, V. M. Gold Nanoparticle Platforms as Drug and Biomacromolecule Delivery Systems. *J. Controlled Release* **2010**, *148*, 122−127.
(6) Boccalon, M.; Bidoggia, S.; Romano, F.; Gualandi, L.; Franchi, P.; Lucarini, M.; Pengo, P.; Pasquato, L. Gold Nanoparticles as Drug Carriers: A Contribution to the Quest for Basic Principles for Monolayer Design. *J. Mater. Chem. B* **2015**, *3*, 432−439.
(7) Jiang, X.; Feng, D.-Q.; Liu, G.; Fan, D.; Wang, W. A Fluorescent Switch Sensor for Detection of Anticancer Drug and CtDNA Based on the Glutathione Stabilized Gold Nanoclusters. *Sens. Actuators, B* **2016**, *232*, 276−282.
(8) Liu, C.-P.; Wu, T.-H.; Liu, C.-Y.; Cheng, H.-J.; Lin, S.-Y. Interactions of nitroxide radicals with dendrimer-entrapped Au8-clusters: a fluorescent nanosensor for intracellular imaging of ascorbic acid. *J. Mater. Chem. B* **2015**, *3*, 191−197.
(9) Zhang, Z.; Berg, A.; Levanon, H.; Fessenden, R. W.; Meisel, D. On the Interactions of Free Radicals with Gold Nanoparticles. *J. Am. Chem. Soc.* **2003**, *125*, 7959−7963.
(10) Gozdziewska, M.; Cichowicz, G.; Markowska, K.; Zawada, K.; Megiel, E. Nitroxide-Coated Silver Nanoparticles: Synthesis, Surface Physicochemistry and Antibacterial Activity. *RSC Adv.* **2015**, *5*, 58403−58415.
(11) Scaiano, J. C.; Laferrière, M.; Galian, R. E.; Maurel, V.; Billone, P. Non-Linear Effects in the Quenching of Fluorescent Semiconductor Nanoparticles by Paramagnetic Species. *Phys. Status Solidi A* **2006**, *203*, 1337−1343.
(12) Swiech, O.; Hrynkiewicz-Sudnik, N.; Palys, B.; Kaim, A.; Bilewicz, R. Gold Nanoparticles Tethered to Gold Surfaces Using Nitroxyl Radicals. *J. Phys. Chem. C* **2011**, *115*, 7347−7354.
(13) Zhang, L.; Wang, E. Metal Nanoclusters: New Fluorescent Probes for Sensors and Bioimaging. *Nano Today* **2014**, *9*, 132−157.
(14) Tansakul, C.; Lilie, E.; Walter, E. D.; Rivera, F.; Wolcott, A.; Zhang, J. Z.; Millhauser, G. L.; Braslau, R. Distance-Dependent Fluorescence Quenching and Binding of CdSe Quantum Dots by Functionalized Nitroxide Radicals. *J. Phys. Chem. C* **2010**, *114*, 7793−7805.
(15) Chen, W.; Wang, X.; Tu, X.; Pei, D.; Zhao, Y.; Guo, X. Water-Soluble off-on Spin-Labeled Quantum-Dots Conjugate. *Small* **2008**, *4*, 759−764.
(16) Aliaga, C.; Michea, S.; Pastenes, C.; Salazar, J.; Rezende, M. C. On the Interactions of TEMPO Radicals with Gold Nanostructures. *New J. Chem.* **2018**, *42*, 9764−9770.
(17) Chrétien, S.; Gordon, M. S.; Metiu, H. Binding of Propene on Small Gold Clusters and on Au(111): Simple Rules for Binding Sites and Relative Binding Energies. *J. Chem. Phys.* **2004**, *121*, 3756−3766.
(18) Mollenhauer, D.; Gaston, N.; Voloshina, E.; Paulus, B. Interaction of Pyridine Derivatives with a Gold (111) Surface as a Model for Adsorption to Large Nanoparticles. *J. Phys. Chem. C* **2013**, *117*, 4470−4479.
(19) Zhang, L.; Ren, T.; Zhou, L.; Tian, J.; Li, X. DFT Investigation of the Intermolecular Interactions of a Thieno-Separated Tricyclic Guanine Analog with Gold Nanoclusters. *Comput. Theor. Chem.* **2013**, *1019*, 1−10.
(20) Prakash, M.; Chambaud, G.; Al-Mogren, M. M.; Hochlaf, M. Role of Size and Shape Selectivity in Interaction between Gold Nanoclusters and Imidazole: A Theoretical Study. *J. Mol. Model.* **2014**, *20*, 2534−2546.
(21) Lugo, G.; Schwanen, V.; Fresch, B.; Remacle, F. Charge Redistribution Effects on the UV-Vis Spectra of Small Ligated Gold Clusters: A Computational Study. *J. Phys. Chem. C* **2015**, *119*, 10969−10980.




DOI: 10.1021/acs.jpcc.9b03422
*J. Phys. Chem. C* 2019, 123, 21713−21720

(22) Wang, H.; Li, X.; Gao, L.; Zhai, J.; Liu, R.; Gao, X.; Wang, D.; Zhao, L. Atomic Structure of a Peptide Coated Gold Nanocluster Identified Using Theoretical and Experimental Studies. *Nanoscale* **2016**, *8*, 11454−11460.
(23) Camarada, M. B. PAMAM Dendrimers as Support for the Synthesis of Gold Nanoparticles: Understanding the Effect of the Terminal Groups. *J. Phys. Chem. A* **2017**, *121*, 8124−8135.
(24) Rodríguez-Castillo, M.; Lugo-Preciado, G.; Laurencin, D.; Tielens, F.; van der Lee, A.; Clément, S.; Guari, Y.; López-de-Luzuriaga, J. M.; Monge, M.; Remacle, F.; et al. Experimental and Theoretical Study of the Reactivity of Gold Nanoparticles Towards Benzimidazole-2-Ylidene Ligands. *Chem.—Eur. J.* **2016**, *22*, 10446−10458.
(25) Parr, R. G.; Yang, W. Density Functional Approach to the Frontier-Electron Theory of Chemical Reactivity. *J. Am. Chem. Soc.* **1984**, *106*, 4049−4050.
(26) De, H. S.; Krishnamurty, S.; Pal, S. Understanding the Reactivity Properties of Aun ($6 \leq n \leq 13$) Clusters Using Density Functional Theory Based Reactivity Descriptors. *J. Phys. Chem. C* **2010**, *114*, 6690−6703.
(27) Johnson, E. R.; Keinan, S.; Mori-Sánchez, P.; Contreras-García, J.; Cohen, A. J.; Yang, W. Revealing Noncovalent Interactions. *J. Am. Chem. Soc.* **2010**, *132*, 6498−6506.
(28) Contreras-García, J.; Yang, W.; Johnson, E. R. Analysis of Hydrogen-Bond Interaction Potentials from the Electron Density: Integration of Noncovalent Interaction Regions. *J. Phys. Chem. A* **2011**, *115*, 12983−12990.
(29) Fuentealba, P.; Cárdenas, C. Density Functional Theory of Chemical Reactivity. *Chem. Modell.* **2015**, *11*, 151−174.
(30) Osorio, E.; Ferraro, M. B.; Oña, O. B.; Cardenas, C.; Fuentealba, P.; Tiznado, W. Assembling Small Silicon Clusters Using Criteria of Maximum Matching of the Fukui Functions. *J. Chem. Theory Comput.* **2011**, *7*, 3995−4001.
(31) Frisch, M. J.; Trucks, G. W.; Schlegel, H. B.; Scuseria, G. E.; Robb, M. A.; Cheeseman, J. R.; Scalmani, G.; Barone, V.; Mennucci, B.; Petersson, G. A.; et al. *Gaussian 09*, Revision E.01; Gaussian Inc.: Wallingford CT, 2009.
(32) Lin, Y.-S.; Li, G.-D.; Mao, S.-P.; Chai, J.-D. Long-Range Corrected Hybrid Density Functionals with Improved Dispersion Corrections. *J. Chem. Theory Comput.* **2013**, *9*, 263−272.
(33) Chai, J.-D.; Head-Gordon, M. Systematic Optimization of Long-Range Corrected Hybrid Density Functionals. *J. Chem. Phys.* **2008**, *128*, 084106−084115.
(34) Figgen, D.; Rauhut, G.; Dolg, M.; Stoll, H. Energy-Consistent Pseudopotentials for Group 11 and 12 Atoms: Adjustment to Multi-Configuration Dirac-Hartree-Fock Data. *Chem. Phys.* **2005**, *311*, 227−244.
(35) Peterson, K. A.; Puzzarini, C. Systematically Convergent Basis Sets for Transition Metals. II. Pseudopotential-Based Correlation Consistent Basis Sets for the Group 11 (Cu, Ag, Au) and 12 (Zn, Cd, Hg) Elements. *Theor. Chem. Acc.* **2005**, *114*, 283−296.
(36) Chai, J.-D.; Head-Gordon, M. Long-Range Corrected Hybrid Density Functionals with Damped Atom-Atom Dispersion Corrections. *Phys. Chem. Chem. Phys.* **2008**, *10*, 6615−6620.
(37) Goerigk, L.; Grimme, S. A Thorough Benchmark of Density Functional Methods for General Main Group Thermochemistry, Kinetics, and Noncovalent Interactions. *Phys. Chem. Chem. Phys.* **2011**, *13*, 6670−6688.
(38) Zheng, J.; Petty, J. T.; Dickson, R. M.; Robert, M. High Quantum Yield Blue Emission from Water-Soluble Au8Nanodots. *J. Am. Chem. Soc.* **2003**, *125*, 7780−7781.
(39) Cárdenas, C.; Ayers, P. W.; Cedillo, A. Reactivity Indicators for Degenerate States in the Density-Functional Theoretic Chemical Reactivity Theory. *J. Chem. Phys.* **2011**, *134*, 174103−174119.
(40) Bultinck, P.; Cardenas, C.; Fuentealba, P.; Johnson, P. A.; Ayers, P. W. How to Compute the Fukui Matrix and Function for Systems with (Quasi-)Degenerate States. *J. Chem. Theory Comput.* **2014**, *10*, 202−210.
(41) Cárdenas, C.; Muñoz, M.; Contreras, J.; Ayers, P. W.; Gómez, T.; Fuentealba, P. Understanding Chemical Reactivity in Extended Systems: Exploring Models of Chemical Softness in Carbon Nanotubes. *Acta Phys.-Chim. Sin.* **2018**, *34*, 631−638.
(42) Heidar-Zadeh, F.; Richer, M.; Fias, S.; Miranda-Quintana, R. A.; Chan, M.; Franco-Pérez, M.; González-Espinoza, C. E.; Kim, T. D.; Lanssens, C.; Patel, A. H. G.; et al. An Explicit Approach to Conceptual Density Functional Theory Descriptors of Arbitrary Order. *Chem. Phys. Lett.* **2016**, *660*, 307−312.
(43) Serapian, S. A.; Bearpark, M. J.; Bresme, F. The Shape of Au8: Gold Leaf or Gold Nugget? *Nanoscale* **2013**, *5*, 6445−6457.
(44) Johansson, M. P.; Warnke, I.; Le, A.; Furche, F. At What Size Do Neutral Gold Clusters Turn Three-Dimensional? *J. Phys. Chem. C* **2014**, *118*, 29370−29377.
(45) Shafai, G.; Hong, S.; Bertino, M.; Rahman, T. S. Effect of Ligands on the Geometric and Electronic Structure of Au13 Clusters. *J. Phys. Chem. C* **2009**, *113*, 12072−12078.


DOI: 10.1021/acs.jpcc.9b03422
*J. Phys. Chem. C* 2019, 123, 21713−21720